Issues in the inverse modeling of a single ring infiltration experiment

Michal Kuraz[a], Lukas Jacka[a], Johanna Ruth Bloecher[a], Matej Leps[b]

[a]*Czech University of Life Sciences Prague, Faculty of Environmental Sciences, Department of Water Resources and Environmental Modeling*
[b]*Czech Technical University in Prague, Faculty of Civil Engineering, Department of Mechanics*

Abstract

This contribution addresses issues in the identification of soil hydraulic properties (SHP) obtained from inverse modeling of a single ring (SR) infiltration experiment. The SR experimental data were obtained from a series of in situ experiments conducted on a highly heterogeneous mountainous podzolic soil profile. The main purpose of this inverse analysis was to evaluate the SHP parameterized with the van Genuchten model, and to answer to what extent the well-known SR experiment is robust enough to provide a unique estimate of these parameters.

The SHP of the topsoil layer are very difficult to measure directly, since the thickness of the top soil layer is often much smaller than the depth required to embed the SR or Guelph permeameter device or to obtain undisturbed samples for further laboratory experiments.

We investigated the question whether is it possible to characterize the unsteady part of the SR infiltration experiment with a unique set of parameters representing SHP, and whether all parameters are vulnerable to non-uniqueness. To evaluate non-uniqueness, local optima were identified and mapped using the simplified atavistic differential evolution algorithm (Hrstka and Kučerová, 2004; Ibrahimbegović et al., 2004).

We also discuss important issues regarding (i) the design of the numerical simulations, (ii) the influence of spatial and temporal discretization on the identified local optima and (iii) convergence issues with the nonlinear operator.

Keywords: soil hydraulic properties, inverse modeling of the Richards equation, FEM approximation of the Richards equation, differential evolution, application of dd-adaptivity algorithm, computational hydrology, computational soil science

1. Introduction

Soil hydraulic properties (hereafter SHP) are important for many hydrological models and engineering applications. The mountainous podzolic soil evaluated here is typical for the source areas of many major

rivers in the Central European region. The top layer of the soil plays a key role in the rainfall-runoff process, because it is the top-soil that separates the rainfall into surface runoff and subsurface runoff.

Due to the rocks present and the dense root system of the covering vegetation, and due to the possible extension of the representative elementary volume, it is often impossible to collect undisturbed samples of top-soil for laboratory measurements in order to obtain the SHP parameters (Jačka et al., 2014). The SHP of the topsoil are therefore very difficult to measure directly (Fodor et al., 2011; Jačka et al., 2014).

In our study, the well-known single ring (hereafter SR) method was used to obtain experimental input data (cumulative infiltration) for inverse modeling. The SR infiltrometer is a widely accepted, simple, robust field method, which is able to measure infiltration process, which affects the entire soil profile including the top-soil, and can sample a relatively large volume (depending on the diameter of the ring) (Cheng et al., 2011; Reynolds, 2008a). The SR infiltration experiment is an in situ experiment, which does not require soil samples to be collected, so the porous medium is kept relatively undisturbed. With the widely-used ring diameter of 30 cm, the affected porous media is far more representative than any soil sample we were able to collect. The top-soil can also be measured (with some alteration of the surface) using other well-known field infiltration methods, e.g. the tension infiltrometer or the well permeameter (Angulo-Jaramillo et al., 2000; Reynolds, 2008b).

The Richards equation (Richards, 1931) describes flow in variably saturated porous media. In order to model environmental processes and engineering applications with the Richards equation knowledge of the SHP is essential. SHP can be summarized by the soil water retention curve and soil hydraulic conductivity curve. In this contribution, the SHP are parametrized with the frequently used Mualem-van Genuchten model (van Genuchten, 1980). We refer to this model as REVG.

Several studies compared REVG inverse modeling of tension infiltrometers (Simunek et al., 1998, 1999; Schwartz and Evett, 2002; Ventrella et al., 2005; Ramos et al., 2006; Verbist et al., 2009; Rezaei et al., 2016). They state that the retention curves obtained from inverse modeling using tension infiltrometer data are often not in good agreement with laboratory experiments on undisturbed samples. In particular, the saturated water content obtained from an inverse model of REVG is typically distinctly lower than the experimentally established value (Simunek et al., 1998; Verbist et al., 2009). There are various theories explaining the issue to be due to (i) the effect of hysteresis as the drying process in the laboratory differs from the wetting process in the field, (ii) the effect of entrapped air in the field (Fodor et al., 2011), where the saturation may not fully correspond to the pressure head, and (iii) the effect of macropores, which are excluded when a tension infiltrometer is used. Most importantly the soil samples usually examined in the

laboratory are typically much smaller than the representative elementary volume (Scharnagl et al., 2011). However, several studies reported a close correspondence between the retention curve parameters obtained from laboratory experiments and from REVG analyses (Ramos et al., 2006; Schwartz and Evett, 2002). The identification of SHP from transient infiltration experiments has been a subject of numerous publications in past decades (Inoue et al., 2000; Lassabatère et al., 2006; Kohne et al., 2006; Xu et al., 2012; Bagarello et al., 2017; Younes et al., 2017). Inoue et al. (2000) reported a close correspondence between the SHP obtained from the inverse modeling of dynamic transient infiltration experiments with those obtained from steady-state laboratory experiments, where the uniqueness of the inverse model was preserved by considering the dynamically changing pressure head, water content and even tracer concentration.

The non-uniqueness of the REVG inverse model is already a very well-known issue, and has been described by a number of publications over the last decades (Kool et al., 1985; Mous, 1993; Hwang and Powers, 2003; Binley and Beven, 2003). **However, we have not succeeded in our search for more recent contributions in this field.** Mous (1993) defined criteria for model identifiability based on the sensitivity matrix rank, however numerical computation of the sensitivity matrix, which is defined by the derivatives of the objective function, often involves difficulties in managing truncation and round-off errors. Binley and Beven (2003) demonstrated on a real world case study of Sherwood Sandstone Aquifer that many different SHP parameters of macroscopic media can represent the layered unsaturated zone and provide acceptable simulations of the observed aquifer recharges. Mous (1993) explained that in case of the absence of water content data, the residual water content should be excluded from the identification to avoid non-uniqueness. However, Binley and Beven (2003) used a non-unique definition where both the unknown residual and saturated water content were considered. The definition of a unique inverse function for identification of macroscopic media was treated in (Zou et al., 2001), where the recommended approach was to assemble the objective function from transient data of the capillary pressure and from the steady state water content data.

must be checked!!

Another challenging issue is the treatment of the nonlinear operator of the Richards equation. Binley and Beven (2003) reported that 56% of the simulations were rejected during Monte Carlo simulations on a wide range of parameters, because of convergence problems. Their study did not mention explicitly why. We assume that these convergence issues originated from the nonlinear operator treatment – the outer iterations. It could be concluded, that if we use a simple Picard method for the nonlinear operator, and we increase the iteration criterion (which is typically referred to as h or θ tolerance), we will obtain a less accurate solution but we will also need less iterations for the Picard method. If we increase the criterion enough, we end up

with a semi-implicit solution, where the constitutive functions in the Richards equation are evaluated from the previous time level solution – thus we just need a single outer iteration.

The following questions arise:

- Is it possible to approximate the unsteady SR experiment using the REVG model, where the only unknown parameters represent the thin topsoil layer, by a unique set of parameters?
- If not, are all parameters vulnerable to non-uniqueness?
- Are the parameters identified by inverse analysis of SR infiltration dependent on the treatment of the nonlinear operator of the Richards equation? Is there any benefit in using the accurate Newton or Picard iteration method, which can often lead to slow convergence or even divergence, or can we obtain a reasonable estimate with just the semi-implicit scheme?

The aim of this paper is to answer these questions. We approach these issues using a real-world problem aiming to identify SHP for the top soil layer in the experimental catchment Modrava in the Šumava National Park, Czech Republic. The SHP for lower soil layers were already identified through various field and laboratory experiments and by data processing

2. Methodology

This section is divided into two parts. The first part, section 2.1, is focused on assembling the experimental data, which were later used as input for the inverse model. The site description, the reconstruction of the parameters of the SHP for the lower profiles, and the processing of the experimental data is given.

The second part of the methodology covers issues in the REVG inverse model. Section 2.2 derives governing equations and is given together with notes on the numerical stability of the REVG model for rotational symmetric problems. Section 2.3 discusses issues in creating the domain scheme and selecting appropriate boundary conditions, since it is not always easy to find an agreement between the mathematical model setup and physical interpretation. Section 2.4 concludes with a description of the construction of the objective function, and the methodology of the automatic calibration.

2.1. Obtaining the input data for the inverse problem

2.1.1. Site description and assembling the experimental data

The study site is located in the Šumava National Park, and has been described in (Jačka et al., 2014). The location of the site in a map of Modrava 2 catchment is presented by Jačka et al. (2012). A haplic

podzol with distinct soil horizons is dominant on this site. The mean depths of the podzolic horizons are as follows:

- organic horizon O and humus horizon Ah altogether (the top-soil) 7.5 cm,
- eluvial bleached horizon E 12.5 cm,
- spodic horizons Bhs and Bs 40 cm,
- weathered bedrock C.

The average groundwater table level can be roughly estimated at -280 cm below the surface.

The soil characteristics of the horizons below the top-soil are given in the table 1.

I don't get the percentage, I would probably remove even this table.

Table 1: Fractions of the fine soil (¡ 2 mm) and skeleton (¿ 2 mm) and bulk density of the E and Bhs+Bs horizons.

horizon	clay	silt	sand	gravel	bulk density
	$< 2\ \mu$m	2 μm – 0.05 mm	0.05 – 2 mm	> 2 mm	g.cm^{-3}
E		68%		32%	1.4
	1%	20%	79%		
Bhs + Bs		70%		30%	1.3
	7%	32%	61%		

2.1.2. Obtaining SHP parameters for lower horizons

Guelph permeameter measurements (GP) were used to estimate the saturated hydraulic conductivity of the lower horizons. The constant head GP method applied here is described in (Jačka et al., 2014). It is well known that pedotransfer functions work well for spodic and eluvial horizons characterized by high percentage of sand, without a distinct structure, and with a bulk density and porosity corresponding to a standard mineral soil. Parameters representing the retention curves for spodic horizons and eluvial horizon below the top-soil were estimated using the soil texture and the bulk density information with pedotransfer function implemented in Rosetta code (Schaap et al., 2001).

The estimated SHP for the lower horizons below the top soil are depicted in table 2.

2.1.3. Obtaining unsteady infiltration data for the top soil

The purpose of this section is to explain the methodology used for obtaining the data for the proposed inverse analysis.

Table 2: Soil hydraulic parameters for the lower horizons.

horizon	GP experiment sites	θ_s [-]	α [m^{-1}]	n [-]	K_s [ms^{-1}]	S_s [m^{-1}]
E	28	0.46	4.65	1.7408	4.4×10^{-6}	0
Bhs + Bs	19	0.47	2.21	1.4494	1.5×10^{-6}	0
C	8	0.50	3.52	4.03	8.5×10^{-6}	0

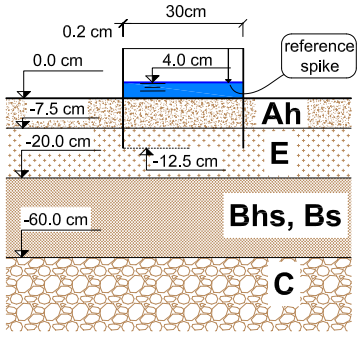

Figure 1: Scheme of the single ring infiltration experiment and the soil layers.

For the O+Ah horizon smoothed experimental data from unsteady single ring (SR) infiltration were used as input for inverse modeling of REVG. The experimental setup was as follows. A steel ring 30 cm in inner diameter, 25 cm in length, and 2 mm in thickness was inserted into the soil to a depth of 12.5 cm, see figure 1. The depth of ponding was kept approximately at a constant level defined by a reference spike, which was placed 4 cm above the surface of the soil. An average experiment duration was 60 minutes.

A total of 22 SR experiments were conducted on the site. The experiments were evaluated as follows. In order to eliminate noise from the experimental values, each SR experiment data set was smoothed. It was observed that the Swartzendruber analytical model (Swartzendruber, 1987) of one-dimensional infiltration exhibited an excellent fitting quality, with the mean Nash-Sutcliffe model efficiency coefficient 0.9974. Thus we made use of exponential data smoothing. The Swartzendruber equation for cumulative infiltration states that

$$I(t) = \frac{c_0\left(1-\exp\left(-c_1\sqrt{t}\right)\right)}{c_1} + c_2 t, \tag{1}$$

where I is the cumulative infiltration $[L]$, and where the parameter set $c_{0,1,2}$, is usually expressed in terms of SHP. This physically based interpretation of the Swartzendruber parameters is disregarded here, since our

infiltration model does not meet the prerequisites for the Swartzendruber model. The Swartzendruber model was considered here as an exponential smoothing and extrapolating function only without any physically based interpretation.

Statistical description of the Swartzendruber parameters and evaluation of the fitting quality of Swartzendruber model is given by (Jačka et al., 2016), see datasets collected on site 3. Representative mean values are as follows: $c_0 = 8.55 \times 10^{-4}$ m.s$^{-0.5}$, $c_1 = 1.13 \times 10^{-1}$ [-], and $c_2 = 5.16 \times 10^{-6}$ m.s^{-1}. The evaluated representative parameter set, together with the model (1), will be used as an input curve for identifying the top soil's SHP. SHP of the lower horizons were already estimated from direct measurements as described in the previous section 2.1.2.

It is already apparent at this stage, that if the infiltration experiment can be well approximated by a three parametric model (1), then the five parametric SHP representation potentially leads to over-parameterization and makes the model non-identifiable (Bellman and Åström, 1970).

2.2. Mathematical model of the field infiltration experiment – governing equation

The field infiltration experiment is characterized by variably saturated conditions ranging between unsaturated and saturated states. It is well known that the flux in porous media under variably saturated conditions can be expressed by the Darcy-Buckingham law (Buckingham, 1907)

$$\mathbf{q} = -\mathbf{K}(\theta)\nabla H, \tag{2}$$

where $\mathbf{q}$ is the volumetric flux [L.T^{-1}], H is the total hydraulic head [L] defined as $H = h + z$, where h is the pressure head [L], z is the potential head [L], θ is the water content [-], and $\mathbf{K}(\theta)$ is the unsaturated hydraulic conductivity [L.T^{-1}]; in general it is a second order tensor. The relation $\theta(h)$ is referred to as the retention curve (van Genuchten, 1980).

The geometry of the flow is inherently three-dimensional, but the domain dimension can be reduced by considering the axisymmetric geometry. The law of mass conservation for incompressible flow in cylindric coordinates is expressed as (Bear, 1979).

$$-\frac{\partial V}{\partial t} = \frac{\partial q_r}{\partial r} + \frac{q_r}{r} + \frac{\partial q_\alpha}{\partial \alpha} + \frac{\partial q_z}{\partial z}, \tag{3}$$

where V is the volume function [-], r is the radial coordinate, α is the angular coordinate, z is the vertical coordinate, and $q_{r,\alpha,z}$ is the volume flux [L.T^{-1}]. The ring infiltration experiment is characterized by

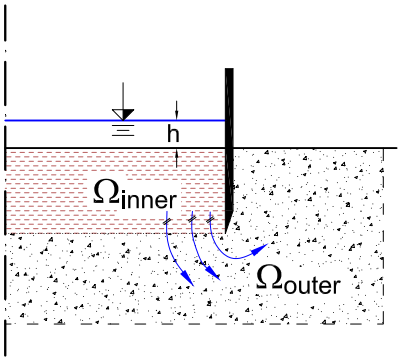

Figure 2: Scheme of the flow domain and the streamlines of infiltration experiment.

rotational symmetric flow, so the angular derivative vanishes. Then the governing equation for variably saturated and rotational symmetric flow is obtained by substituting the flux in (3) by the Darcy-Buckingham law (2). Together with the consideration of linear elasticity for a porous medium the variably saturated axisymmetric flow in isotropic media is governed by

$$\left(\frac{\mathrm{d}\theta}{\mathrm{d}h} + S_s \frac{\theta(h)}{\theta_s}\right) \frac{\partial h}{\partial t} = \frac{\partial K(h)\frac{\partial H}{\partial z}}{\partial z} + \frac{\partial K(h)\frac{\partial H}{\partial r}}{\partial r} + c(\mathbf{x})\frac{\partial H}{\partial r}, \tag{4}$$

where S_s is the specific storage [L^{-1}], θ_s is the saturated water content [-], $c(\mathbf{x})$ is the coefficient of the convection for r coordinate [T^{-1}], which is explained below, and the vector x is a vector of the spatial coordinates $\mathbf{x} = \left(\begin{smallmatrix} r \\ z \end{smallmatrix}\right)$.

Let us consider the model of the infiltration experiment depicted in figure 2. Let the entire flow domain $\Omega = \Omega_{inner} \cup \Omega_{outer}$, where Ω_{outer} is the flow domain outside the infiltration ring and Ω_{inner} is the flow domain within the infiltration ring, exactly as depicted in figure 3. It is apparent that the streamlines inside subdomain Ω_{inner} are parallel, but the streamlines outside the infiltration ring (inside Ω_{outer}) are only axisymmetric. The convection coefficient $c(\mathbf{x})$ is then defined as follows

$$c(\mathbf{x}) = \begin{cases} 0, & \forall \mathbf{x} \in \Omega_{inner} \\ \frac{1}{r}K(h), & \forall \mathbf{x} \in \Omega_{outer}. \end{cases} \tag{5}$$

Note that we should avoid using the coordinates, where $r = 0$.

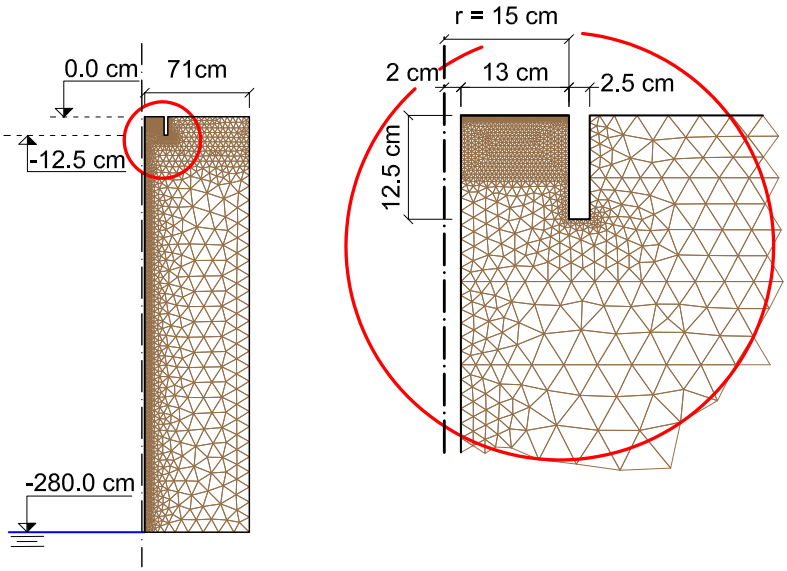

Figure 3: Scheme of the computational domain geometry and domain triangularization.

2.3. Domain scheme, initial conditions and boundary conditions

The goal of the model was to achieve cumulative infiltration – the cumulative flux over the top Dirichlet boundary. The computational domain is depicted in figure 3 together with the discretization mesh. The location of the top boundary was natural – the soil surface. Inside the ring, a Dirichlet condition defines the ponding depth; outside the infiltration ring a Neumann condition defines the no-flow boundary. Locating the bottom boundary was more problematic. The following options are available

- the no-flow boundary (Neumann)
- the free drainage boundary (Neumann)
- the groundwater level - zero pressure head (Dirichlet)

It is apparent that the wetting front originating from our infiltration experiment affects the soil column only to a certain depth. Defining the Neumann no-flow boundary at a sufficient depth would therefore probably not have a significant effect on the derivative of the solution of (4) at the top boundary. At the same time, the only physically acceptable location of the no-flow boundary is the groundwater table. The second option – the free drainage boundary – would be completely incorrect for any depth. The free drainage boundary defines fluxes that probably do not appear in our system at all. Above all, if we consider here the initial

condition as a hydrostatic state, and so

$$\frac{\partial h}{\partial z}(x) = -1, \quad \forall x \in \Omega. \tag{6}$$

The free drainage boundary condition, which is defined as

$$\frac{\partial h}{\partial \mathbf{n}}(x) = 0, \quad \forall (x,t) \in \Gamma_{\text{free drainage}} \times [0,T). \tag{7}$$

is in a conflict with the initial condition (since the outer normal vector $\mathbf{n} = \begin{pmatrix} 0 \\ -1 \end{pmatrix}$), which is again physically incorrect, and produces further computational costs. The reason for the extra computational costs is that the nonlinear equation solver (in this case Picard method) together with the iterative linear equation solver (in this case preconditioned conjugate gradient method) treats iteration increments for the bottom boundary, which is in an ideal case out of the reach of the infiltration experiment. The computational process, that is produced at the bottom boundary in the beginning of the simulation with such boundary setup, originates from the initial and boundary condition mismatch, and has no physical meaning.

It turns out that the only physically correct boundary condition for the bottom boundary is either the Neumann no-flow boundary or Dirichlet boundary both at the groundwater table. The average depth of the groundwater table was known, it is approximately -280 cm below the surface. With this particular setup the domain became extremely narrow and deep, see figure 4.

2.3.1. Stability restrictions of convection dominant problems

The term (5) is the first order derivative term, and so the well known stability restrictions for the numerical solutions of the convection-diffusion problems appear here Christie et al. (1976). The Peclet number representing the numerical stability of convection-diffusion problems is in general given by Knobloch (2008)

$$Pe = \frac{c\Delta x}{2D}, \tag{8}$$

where c is the convection coefficient defined in (5), Δx is the discretization step, and D is the diffusion (for isotropic setup). Based on the definitions given above, equation (8) can be formulated as

$$Pe = \frac{\frac{1}{r}K(h)\Delta x}{2K(h)} = \frac{\Delta x}{2r}. \tag{9}$$

Since our mesh is triangular, Δx can be roughly assumed to be the greatest triangle altitude (since we assume some mesh quality properties). Then a sufficient distance from the axis of anisotropy is such that the Peclet number is sufficiently low. If we want to make our computation free of the well known spurious oscillations Christie et al. (1976); Roos et al. (1996), a sufficiently low Peclet number $Pe \leq 1$ si required. Therefore, the distance from the axis of anisotropy is given by the domain discretization step at the left hand side boundary. The selected discretization step at the left hand side boundary was assumed as $\Delta x = 2$ cm. The domain was therefore detached by 2 cm from the axis of anisotropy, and thus the Peclet number was 0.5 only.

2.3.2. Domain shape restrictions

Since Dusek et al. (2009) mentioned several difficulties with incorrect triangular mesh setup while modeling the SR experiment, we tried to avoid possible numerical issues connected with domains with sharp spikes.

The governing equation (4) will be solved here by linear finite element method, which is a subset of variational methods. Using standard setup the solution H of (4) will be taken from Sobolev functional space defined for functions on Lipschitz bounded domains (Braess, 1997; Rektorys et al., 2000).

In order to avoid the non-Lipschitz boundary (or any boundary with a shape that is close to the non-Lipschitz boundary) the infiltration ring thickness was oversized to 2.5 cm. It is obvious that the real ring thickness is much smaller (in our case 2 mm), but using the real ring thickness yields possible numerical issues, since then the domain becomes a typical case of a non-Lipschitz bounded domain Braess (1997). It is expected, that oversizing the ring thickness does not significantly affect the solution at the top Dirichlet boundary.

2.3.3. Initial and boundary condition setup

As discussed in **??** the left hand side boundary was located at $r = 2$ cm. The right hand side boundary was located at a distance $r = 73$ cm, it means 50 cm from the infiltration ring.

The locations of the domain boundaries are depicted in figure 4. The boundary conditions are specified as follows

$$\begin{aligned} &h(x,t) = 4 \text{ cm} \Rightarrow H(x,t) = 4 \text{ cm}; \quad \forall (x,t) \in \Gamma_1 \times [0,T), \\ &\frac{\partial H}{\partial \mathbf{n}} = 0; \quad \forall (x,t) \in \Gamma_2 \times [0,T), \\ &h(x,t) = 0 \text{ cm } \Rightarrow \ H(x,t) = -280.0 \text{ cm}; \quad \forall (x,t) \in \Gamma_3 \times [0,T). \end{aligned} \tag{10}$$

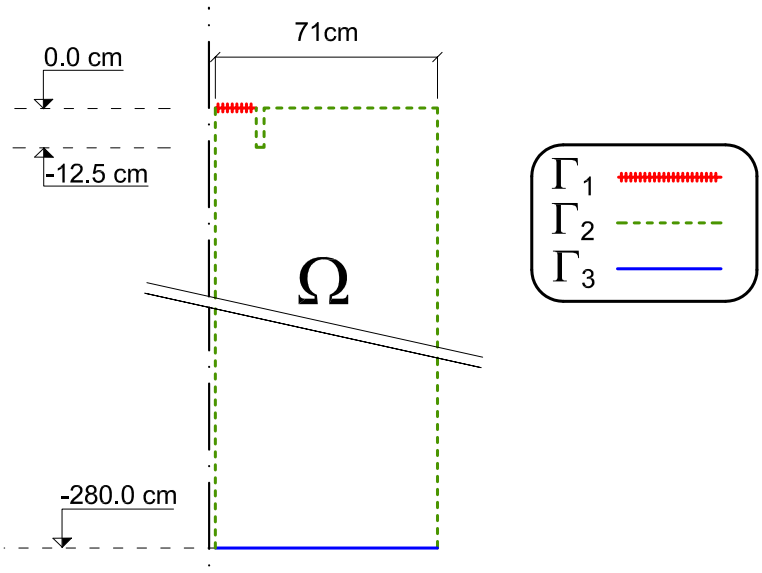

Figure 4: Scheme of the computational domain geometry and the domain boundaries.

where T is the simulation end time $[T]$, and $\mathbf{n}$ is the boundary normal vector.

The initial condition was assumed as a steady state solution of (4) with the boundary $\Gamma_1 \cup \Gamma_2$ assumed as a no-flow boundary – thus the entire domain Ω was considered in a hydrostatic state. Then the initial condition states that

$$H(x) = -280.0 \text{ cm}; \quad \forall x \in \Omega, \tag{11}$$

and thus $\frac{\partial h}{\partial z} = -1$.

2.3.4. Numerical solution, temporal and spatial discretization, automatic calibration methodology

Equation (4) was implemented into the DRUtES library (Kuraz and Mayer, 2008). It is an object-oriented library written in Fortran 2003/2008 standard for solving nonlinear coupled convection-diffusion-reaction type problems. The problem was approximated by the linear finite element method for spatial derivatives and Rothe's method for temporal derivatives. The nonlinear operator was treated with the Schwarz-Picard method – an adaptive domain decomposition (*dd*-adaptivity) – with the ability to activate and deactivate subregions of the computational domain sequentially (Kuraz et al., 2013a, 2014, 2015).

The domain was non-uniformly discretized by a triangular mesh. The smallest spatial step was considered for the top layers inside the infiltration ring, close to the Dirichlet boundary. The mesh is depicted on figure 3. The minimum spatial length was 0.5 cm, and the maximum spatial length was 20 cm. The domain was discretized with 2097 nodes and 3861 elements. The coarse mesh for the *dd*-adaptivity method was a

uniform quadrilateral mesh with elements 17.75×28.0 cm, i.e. a total of 40 coarse elements and 55 nodes. The purpose of the coarse mesh is to organize the elements of the domain triangularization into so-called clusters, which form a basic unit for the adaptive domain decomposition used here for solving the nonlinear problem, details can be found in (Kuraz et al., 2015).

The spatial and temporal discretization of (4) leads to sequential solutions of systems of non-linear equations, see e.g. (Kuraz et al., 2013a). The system was linearized as discussed in Kuraz and Mayer (2013); Kuraz et al. (2013b), and so the numerical solution requires an iterative solution of

$$\mathbf{A}(\mathbf{x}_l^k)\mathbf{x}_l^{k+1} = \mathbf{b}(\mathbf{x}_l^k), \tag{12}$$

where k denotes the iteration level, and l denotes the time level, until

$$||\mathbf{x}_l^{k+1} - \mathbf{x}_l^k||_2 < \varepsilon, \tag{13}$$

where ε is the desired iteration criterion. The iterations required for (12) to converge are denoted as the outer iterations. It is apparent that the number of required outer iterations depends on the ε criterion.

The method (12) degenerates into a kind of semiexplicit approximation if the error criterion ε was taken from the extended real numbers, $\varepsilon \in \overline{\mathbb{R}}$, and assigned as $\varepsilon = +\infty$. This semiexplicit approximation is denoted as

$$\mathbf{A}(\mathbf{x}_{l-1})\mathbf{x}_l = \mathbf{b}(\mathbf{x}_{l-1}). \tag{14}$$

This semiexplicit method always requires just a single outer iteration. With a short time step the method converges to the exact solution. For inappropriate time steps, the method diverges from the exact solution faster than the method (12). Nonetheless, the method (14) is free of possible issues related to the convergence of the nonlinear operator.

The infiltration flux is obtained from the numerical derivative of the solution of (4), and it is well known that inaccurate approximation of the capacity term (time derivative term) yields inaccurate mass properties (Celia et al., 1990). We are aware of the possible impact of spatial and temporal discretization on the identified SHP values. We are also aware of possible difficulties with convergence of the linearized discrete system (12) for certain combinations of SHP parameters during the automatic calibration, as discussed in Binley and Beven (2003). Thus the following methodology for the automatic calibration was proposed here.

(**i**) Proceed the calibration procedure with the quasi-explicit stable numerical technique for treating the nonlinear operator explained in equation (14), with the initial time step $t_{init} = 10^{-6}$ hrs, and for each subsequent time level l, $\Delta t_l = 1.05\Delta t_{l-1}$, where $l = \{1, n_t\}$, where n_t is the number of time levels used for the temporal discretization. The ranges of parameters for this calibration are given in table 3, so the maximal values of SHP are defined as a vector $\mathbf{p}_{r_f,max}$, and the minimal values are defined as a vector $\mathbf{p}_{r_f,min}$. So initially the ranges are extremely broad and exceeding even the physically acceptable values. The spatial discretization for this step of calibration was given in the beginning of this section – 2097 nodes and 3861 elements. Let us assume that this discretization is given by a mesh density function $\Delta(\mathbf{x})^{r_f}$. The function $\Delta(\mathbf{x})^{r_f}$ is understood as a spatial distribution of mesh size density, which was used as an input for the mesh generator T3D (Rypl, 2004). The superscript r_f defines the refinement level, where $r_f = 0$ at this initial stage, and the vector $\mathbf{x}$ refers to spatial coordinates inside the domain Ω.

(**ii**) Let us pressume that this inverse model will have more than just a single solution.

- Then this calibration will generate vectors of SHP values $\mathbf{p}^{i_e}_{r_f}$, where the superscript $i_e = \{1, ..., n_e\}$, where n_e denotes the number of local extremes.

(**iii**) To validate the inverse modeling results, select physically acceptable local extremes with good fitting qualities, and create a scatter plot of the objective function in the local extreme neighborhood with improved temporal integration and spatial discretization. For each $\mathbf{p}^{i_e}_{r_f}$ from the acceptable solutions the neighborhood is defined as

$$\begin{aligned} \mathbf{p}^{i_e}_{r_f,max} &= 1.25\mathbf{p}^{i_e}, \\ \mathbf{p}^{i_e}_{r_f,min} &= 0.75\mathbf{p}^{i_e}. \end{aligned} \tag{15}$$

The improvement of the numerical treatment will be processed as follows:

Increase the discretization level

$$r_f = r_f + 1, \tag{16}$$

and update the following parameters of the numerical treatment

$$\begin{aligned} \Delta(\mathbf{x})^{r_f} &= \frac{\Delta(\mathbf{x})^{r_f-1}}{2}, \\ \varepsilon^{r_f} &= 10^{-3}\ \text{cm} \quad \text{if } r_f = 1, \ \text{ else } \quad \varepsilon^{r_f} = \frac{\varepsilon^{r_f-1}}{10}, \\ t_{init}^{r_f} &= \frac{t_{init}^{r_f-1}}{10}\ \text{hrs}. \end{aligned} \tag{17}$$

If $r_f > 0$, then the nonlinear problem represented now by (12) will be solved by the Schwarz-Picard method – an adaptive domain decomposition (Kuraz et al., 2015). To validate the inverse model solution for $r_f - 1$ discretization level perform the following:

(a) Compare the scatter plots for the selected local extreme i_e created with discretization r_f and $r_f - 1$. For this local extreme a vector of SHP parameters $\mathbf{p}_{r_f-1}^{i_e}$ is handled.

(b) **If** the optima refer to siginificantly different SHP parameters.

- Proceed the calibration again with the new parameter range defined as $\mathbf{p}_{max} = 1.1\mathbf{p}_{r_f-1}^{i_e}$ and $\mathbf{p}_{min} = 0.9\mathbf{p}_{r_f-1}^{i_e}$. This new calibration will update the vector $\mathbf{p}_{r_f-1}^{i_e}$ to $\mathbf{p}_{r_f}^{i_e}$.
- Increase the discretization level r_f as $r_f = r_f + 1$, perform the update (17), return to (**iii**)a, and check the condition (**iii**)b.

(c) **else**

- Exit the calibration process.

In the second stage the unknown SHP parameters will be reduced and the automatic calibration using the initial mesh together with the simple quasi-explicit approximation (14) will proceed. The unknown SHP parameters will be sequentially reduced in the following order until just a single extreme will be identified.

(**I**) S_s – specific storage is often neglected for the unsaturated zone, and thus for the first unknown parameter reduction will be assigned $S_s = 0\ \text{m}^{-1}$

(**II**) θ_s – water content is often easy to measure directly, despite there are no available data for top soil layer, let's presume $\theta_s = 0.6$.

(**III**) K_s – if the identifiability of the inverse model will require also reduction of K_s, then this inverse task became inappropriate for any further analyses, and the conducted SR measurements will be declared as non-identifiable setup for SHP parameters.

The following sections will further explain the definition of the objective function and the parameter identification algorithm.

2.4. Parameter identification, a definition of the objective function

The soil hydraulic parameters (SHP) of the top soil that will be identified were specified in section **??**. Since the parameters will be identified using a stochastic method, we have to introduce a physically reasonable range for each parameter. The ranges for the SHPs are specified in table 3.

Table 3: Ranges of SHPs ($\mathbf{p}_{max}$ and $\mathbf{p}_{min}$) for identifying the SHPs in the top-soil layer for *refinement level* $r_f = 0$. Note that the initial ranges are extremly broad especially for the saturated water content θ_s. This broad range was selected in order to explore the uniqnuess of the REVG inverse model of SR experiment even beyond the physically acceptable solutions.

θ_s [-]	α [m^{-1}]	n [-]	K_s [$\mathrm{m.s}^{-1}$]	S_s [$\mathrm{m}^{-}1$]
0.25 – 0.90	0.01 – 5.0	1.05 – 2.10	10^{-7} – 10^{-4}	0.0 – 10.0

The objective function is defined in the following paragraph.

Let $\bar{I}(\mathbf{p}, t)$ be the cumulative infiltration obtained from solving the mathematical model (4) bounded by the initial and boundary conditions defined in section 2.3 for a certain vector of SHPs parameters $\mathbf{p}$ considered as

$$\bar{I}(\mathbf{p}, t) = \frac{\int_0^t \int_{\Gamma_1} -K \frac{\partial H}{\partial \mathbf{n}}(t) \mathrm{d}\Gamma_1 \mathrm{d}t}{\int_{\Gamma_1} \mathrm{d}\Gamma_1}. \tag{18}$$

Let $I(t)$ be the cumulative infiltration defined by (1) with parameters given in section 2.1.3. Then the objective function was defined for three different criteria in order to avoid ill-posed objective function definition.

The objective functions were defined as follows:

I. First criterion Ψ_1 was defined as L_2 norm of the difference between the experimental and model data and thus

$$\Psi_1(\mathbf{p}) = \sqrt{\int_0^{T_{end}} \left(\bar{I}(\mathbf{p}, t) - I(t)\right)^2 \mathrm{d}t}, \tag{19}$$

where T_{end} is the final simulation time $[T]$, which is indeed the root mean square error for continous functions. The meaning of the integrals in nominator and denominator is that the average cummulative infiltration accross the Dirichlet boundary is taken.

II. Second criterion was the L_∞ norm of the difference between the experimental and model data and thus

$$\Psi_2(\mathbf{p}) = \sup\left(\sqrt{\left(\bar{I}(\mathbf{p},t) - I(t)\right)^2}\right), \quad t \in (0, T_{end}). \tag{20}$$

III. Third criterion was considered as the difference between the infiltration rates (final derivatives) between the model data and the experimental data

$$\Psi_3(\mathbf{p}) = \sqrt{\left(\frac{\mathrm{d}\bar{I}(\mathbf{p},T_{end})}{\mathrm{d}t} - \frac{\mathrm{d}I(T_{end})}{\mathrm{d}t}\right)^2}. \tag{21}$$

And so we have applied here a multi-objective optimization. However, it is apparent that minimizing the objective function (19) also minimizes the objective functions (20) and (21). The aim of this multi-objective definition was improving the conditioning of this inverse problem. If we considered the objective function (19) only, then we were probably able to obtain the same solution as with this multi-objective definition with slower convergence of optimization procedure only (the selection of the optimization algorithm will be explained in the following section 2.4.1). This multi-objective function definition is based on experience from our previous attempts in inverse analyses of this infiltration problem.

2.4.1. Optimization method

The most traditional way of dealing of multiple objectives in optimization is the Weighted Sum Method (WSF). Each objective out of kk objectives $f_i(\mathbf{x})$ is multiplied by user defined weights w_i and their sum is optimized. The problem is converted into single criteria optimization:

$$F(\mathbf{x}) = \sum_{i=1}^{kk} w_i f_i(\mathbf{x}), \qquad \sum_{i=1}^{kk} w_i = 1, \quad w_i \geq 0, \tag{22}$$

and any single-objective optimization method can be used to solve (22). Although this method is really easy and intuitive, the biggest obstacle is in setting the weights. The weights express the relative importance of individual objectives, which, in real world applications, is difficult to determine. The success of the WSM depends also on scaling of objectives; all of them should have more or less the same order of magnitude to affect the value of $F(\mathbf{x})$ similarly. Therefore, not only weight vector must be set, but also a normalization of objectives must be performed. Similarly to weight vector, it is difficult to determine in advance which objectives' values can be reached and accordingly, to properly set the normalization vector.

It seems to be advantageous to use population-based Evolutionary Algorithms to obtain the Pareto set for general multi-objective optimization problem.

In this contribution, a genetic algorithm called GRADE (Ibrahimbegović et al., 2004; Kucerova, 2007) was applied. It is a real-coded genetic algorithm combining the ideas of genetic operators: cross-over, mutation and selection taken from the standard genetic algorithm and the idea of differential operator taken from the differential evolution. Moreover, the algorithm GRADE is supported with the niching method CERAF, which was developed based on an idea of enhancing the algorithm with memory and restarts (Hrstka and Kucerova, 2004). When the GRADE algorithm loses the convergence, the current position of the optimization algorithm is marked as a local extreme and a forbidden area is build around in order to forbid the optimization algorithm again to fall into the same local extreme. Hence all inspected local extremes are stored in memory and can be inspected after the optimization.

The main setting of the optimization procedure was as follows: the population of the genetic algorithm contains 30 independent solutions, the whole identification stops after 20.000 objective function evaluations and a local extreme was marker after 600 evaluations without any improvement.

3. Results and discussion

4. Conclusions

5. Acknowledgement

Financial support from the Czech Science Foundation (research project GACR 13-11977P) is gratefully acknowledged.

References

Angulo-Jaramillo, R., Vandervaere, J.P., Roulier, S., Thony, J.L., Gaudet, J.P., Vauclin, M., 2000. Field measurement of soil surface hydraulic properties by disc and ring infiltrometers: A review and recent developments. Soil Tillage Res. 55, 1–29. doi:10.1016/S0167-1987(00)00098-2.

Bagarello, V., Prima, S.D., Iovino, M., 2017. Estimating saturated soil hydraulic conductivity by the near steady-state phase of a beerkan infiltration test. Geoderma 303, 70 – 77. URL: http://www.sciencedirect.com/science/article/pii/S001670611730201X, doi:https://doi.org/10.1016/j.geoderma.2017.04.030.

Bear, J., 1979. Hydraulics of groundwater. McGraw-Hill series in water resources and environmental engineering, McGraw-Hill International Book Co.

Bellman, R., Åström, K., 1970. On structural identifiability. Mathematical Biosciences 7, 329 – 339. URL: http://www.sciencedirect.com/science/article/pii/002555647090132X, doi:https://doi.org/10.1016/0025-5564(70)90132-X.

Binley, A., Beven, K., 2003. Vadose zone flow model uncertainty as conditioned on geophysical data. Ground Water 41, 119–127. URL: http://dx.doi.org/10.1111/j.1745-6584.2003.tb02576.x, doi:10.1111/j.1745-6584.2003.tb02576.x.

Braess, D., 1997. Finite elements: Theory, fast solvers, and applications in solid mechanics. Cambridge University Press.

Buckingham, E., 1907. Studies on the movement of soil moisture. USDA Bureau of Soils – Bulletin 38.

Celia, M.A., Bouloutas, E.T., Zarba, R.L., 1990. A general mass-conservative numerical solution for the unsaturated flow equation. Water Resources Research 26, 1483–1496. doi:10.1029/WR026i007p01483.

Cheng, Q., Chen, X., Chen, X., Zhang, Z., Ling, M., 2011. Water infiltration underneath single-ring permeameters and hydraulic conductivity determination. J. Hydrol. 398, 135–143. doi:10.1016/j.jhydrol.2010.12.017.

Christie, I., Griffiths, D.F., Mitchell, A.R., Zienkiewicz, O.C., 1976. Finite element methods for second order differential equations with significant first derivatives. International Journal for Numerical Methods in Engineering 10, 1389–1396. URL: http://dx.doi.org/10.1002/nme.1620100617, doi:10.1002/nme.1620100617.

Dusek, J., Dohnal, M., Vogel, T., 2009. Numerical analysis of ponded infiltration experiment under different experimental conditions. Soil and Water Research 4, 22–27.

Fodor, N., Sándor, R., Orfánus, T., Lichner, L., Rajkai, K., 2011. Evaluation method dependency of measured saturated hydraulic conductivity. Geoderma 165, 60–68. doi:10.1016/j.geoderma.2011.07.004.

van Genuchten, M., 1980. Closed-form equation for predicting the hydraulic conductivity of unsaturated soils. Soil Science Society of America Journal 44, 892–898. URL: http://www.scopus.com/inward/record.url?eid=2-s2.0-0019057216&partnerID=40&md5=1a9a45e1c2b571c00ebb9a9f9ebaaf92.

Hrstka, O., Kucerova, A., 2004. Improvements of real coded genetic algorithms based on differential operators preventing premature convergence. Advances in Engineering Software 35, 237 – 246. doi:http://dx.doi.org/10.1016/S0965-9978(03)00113-3.

Hrstka, O., Kučerová, A., 2004. Improvements of real coded genetic algorithms based on differential operators preventing premature convergence. Advances in Engineering Software 35, 237 – 246. URL: http://www.sciencedirect.com/science/article/pii/S0965997803001133, doi:https://doi.org/10.1016/S0965-9978(03)00113-3.

Hwang, S.I., Powers, S.E., 2003. Estimating unique soil hydraulic parameters for sandy media from multi-step outflow experiments. Advances in Water Resources 26, 445 – 456. URL: http://www.sciencedirect.com/science/article/pii/S0309170802001070, doi:https://doi.org/10.1016/S0309-1708(02)00107-0.

Ibrahimbegović, A., Knopf-Lenoir, C., Kucerova, A., Villon, P., 2004. Optimal design and optimal control of structures undergoing finite rotations and elastic deformations. International Journal for Numerical Methods in Engineering 61, 2428–2460.

Inoue, M., Šimøunek, J., Shiozawa, S., Hopmans, J., 2000. Simultaneous estimation of soil hydraulic and solute transport parameters from transient infiltration experiments. Advances in Water Resources 23, 677 – 688. URL: http://www.sciencedirect.com/science/article/pii/S0309170800000117, doi:https://doi.org/10.1016/S0309-1708(00)00011-7.

Jačka, L., Pavlásek, J., Jindrová, M., Bašta, P., Černý, M., Balvín, A., Pech, P., 2012. Steady infiltration rates estimated for a mountain forest catchment based on the distribution of plant species. J. For. Sci. 58, 536–544.

Jačka, L., Pavlásek, J., Kuráž, V., Pech, P., 2014. A comparison of three measuring methods for estimating the saturated hydraulic conductivity in the shallow subsurface layer of mountain podzols. Geoderma 219–220, 82 – 88. doi:10.1016/j.geoderma.2013.12.027.

Jačka, L., Pavlásek, J., Pech, P., Kuráž, V., 2016. Assessment of evaluation methods using infiltration data measured in heterogeneous mountain soils. Geoderma 276, 74 – 83. URL: http://www.sciencedirect.com/science/article/pii/S0016706116301823, doi:http://dx.doi.org/10.1016/j.geoderma.2016.04.023.

Knobloch, P., 2008. On the choice of the supg parameter at outflow boundary layers. Advances in Computational Mathematics 31, 369. URL: https://doi.org/10.1007/s10444-008-9075-6, doi:10.1007/s10444-008-9075-6.

Kohne, J., Mohanty, B., Simunek, J., 2006. Inverse dual-permeability modeling of preferential water flow in a soil column and implications for field-scale solute transport. Vadose zone journal 5, 59 – 76. doi:http://dx.doi.org/10.2136/vzj2005.0008.

Kool, J., Parker, J., Van Genuchten, M., 1985. Determining soil hydraulic properties from one-step outflow experiments by parameter estimation. i. theory and numerical studies. Soil Science Society of America 49, 1348 – 1354.

Kucerova, A., 2007. Identification of nonlinear mechanical model parameters based on softcomputing methods. Ph.D. thesis. Ecole Normale Supérieure de Cachan, Laboratoire de Mécanique et Technologie.

Kuraz, M., Mayer, P., 2008. Drutes – an opensource library for solving coupled nonlinear convection-diffusion-reaction equations. URL: http://www.drutes.org.

Kuraz, M., Mayer, P., 2013. Algorithms for solving darcian flow in structured porous media. Acta Polytecnica 53, 347–358.

Kuraz, M., Mayer, P., Havlicek, V., Pech, P., 2013a. Domain decomposition adaptivity for the richards equation model. Computing 95, 501–519. URL: http://dx.doi.org/10.1007/s00607-012-0279-8, doi:10.1007/s00607-012-0279-8.

Kuraz, M., Mayer, P., Havlicek, V., Pech, P., Pavlasek, J., 2013b. Dual permeability variably saturated flow and contaminant transport modeling of a nuclear waste repository with capillary barrier protection. Applied Mathematics and Computation 219, 7127 – 7138. doi:http://dx.doi.org/10.1016/j.amc.2011.08.109.

Kuraz, M., Mayer, P., Pech, P., 2014. Solving the nonlinear richards equation model with adaptive domain decomposition. Journal of Computational and Applied Mathematics 270, 2 – 11. URL: http://www.sciencedirect.com/science/article/pii/S0377042714001502, doi:http://dx.doi.org/10.1016/j.cam.2014.03.010. fourth International Conference on Finite Element Methods in Engineering and Sciences (FEMTEC 2013).

Kuraz, M., Mayer, P., Pech, P., 2015. Solving the nonlinear and nonstationary richards equation with two-level adaptive domain decomposition (dd-adaptivity). Applied Mathematics and Computation 267, 207 – 222.

Lassabatère, L., Angulo-Jaramillo, R., Soria Ugalde, J.M., Cuenca, R., Braud, I., Haverkamp, R., 2006. Beerkan estimation of soil transfer parameters through infiltration experiments–best. Soil Science Society of America Journal 70, 521 – 532. doi:http://dx.doi.org/10.2136/sssaj2005.0026.

Mous, S., 1993. Identification of the movement of water in unsaturated soils: the problem of identifiability of the model. Journal of Hydrology 143, 153 – 167. URL: http://www.sciencedirect.com/science/article/pii/0022169493900930, doi:https://doi.org/10.1016/0022-1694(93)90093-0. xVI General Assembly of the European Geophysical Society.

Ramos, T., Goncalves, M., Martins, J., van Genuchten, M., Pires, F., 2006. Estimation of soil hydraulic properties from numerical inversion of tension disk infiltrometer data. VADOSE ZONE JOURNAL 5, 684–696. doi:10.2136/vzj2005.0076.

Rektorys, K., Cipra, T., Drabek, K., Fiedler, M., Fuka, J., Kejla, F., Kepr, B., Nevas, J., Nozicka, F., Prager, M., Segeth, K., Vilhelm, V., Vitasek, E., Zelenka, M., 2000. Overview of Applied Mathematics I, II. Prometheus, Prague.

Reynolds, W.D., 2008a. Saturated hydraulic properties: Ring infiltrometer, in: Carter M.R., Gregorich, E.G. [Eds.], Soil Sampling and Methods of Analysis, 2nd ed. CRC Press Taylor & Francis, Boca Raton, USA, pp. 1043–1056.

Reynolds, W.D., 2008b. Saturated hydraulic properties: Well permeameter, in: Carter M.R., Gregorich, E.G. [Eds.], Soil Sampling and Methods of Analysis, 2nd ed. CRC Press Taylor & Francis, Boca Raton, USA, pp. 1025–1042.

Rezaei, M., Seuntjens, P., Shahidi, R., Joris, I., Boënne, W., Al-Barri, B., Cornelis, W., 2016. The relevance of in-situ and laboratory characterization of sandy soil hydraulic properties for soil water simulations. Journal of Hydrology 534, 251 – 265. URL: http://www.sciencedirect.com/science/article/pii/S0022169416000044, doi:http://dx.doi.org/10.1016/j.jhydrol.2015.12.062.

Richards, L.A., 1931. Capillary conduction of liquids through porous mediums. Journal of Applied Physics 1, 318–333. doi:10.1063/1.1745010.

509 Roos, H., G., Stynes, M., Tobiska, L., 1996. Numerical Methods for Singularly Perturbed Differential
510 Equations, Convection-Diffusion and Flow Problems. Springer-Verlag Berlin Heidelberg.

511 Rypl, D., 2004. T3D Mesh Generator. Department of Mechanics, CTU in Prague, Czech Republic. Prague,
512 Czech Republic. URL: http://mech.fsv.cvut.cz/~dr/t3d.html.

513 Schaap, M.G., Leij, F.J., van Genuchten, M.T., 2001. rosetta: a computer program for estimating soil
514 hydraulic parameters with hierarchical pedotransfer functions. J. Hydrol. 251, 163 – 176. doi:http:
515 //dx.doi.org/10.1016/S0022-1694(01)00466-8.

516 Scharnagl, B., Vrugt, J.A., Vereecken, H., Herbst, M., 2011. Inverse modelling of in situ soil water dynamics:
517 investigating the effect of different prior distributions of the soil hydraulic parameters. Hydrology and
518 Earth System Sciences 15, 3043–3059. URL: http://www.hydrol-earth-syst-sci.net/15/3043/2011/,
519 doi:10.5194/hess-15-3043-2011.

520 Schwartz, R., Evett, S., 2002. Estimating hydraulic properties of a fine-textured soil using a disc infiltrometer.
521 SOIL SCIENCE SOCIETY OF AMERICA JOURNAL 66, 1409–1423.

522 Simunek, J., van Genuchten, M., T., Gribb, M., Hopmans, J.W., 1998. Parameter estimation of unsaturated
523 soil hydraulic properties from transient flow processes1. Soil Tillage Res. 47, 27 – 36. doi:http://dx.doi.
524 org/10.1016/S0167-1987(98)00069-5.

525 Simunek, J., Wendroth, O., van Genuchten, M., 1999. Estimating unsaturated soil hydraulic properties from
526 laboratory tension disc infiltrometer experiments. WATER RESOURCES RESEARCH 35, 2965–2979.
527 doi:{10.1029/1999WR900179}.

528 Swartzendruber, D., 1987. A Quasi-Solution of Richards Equation for the Downward Infiltration of Water
529 into Soil. Water Resour. Res. 23, 809–817. doi:10.1029/WR023i005p00809.

530 Ventrella, D., Losavio, N., Vonella, A., Leij, F., 2005. Estimating hydraulic conductivity of a fine-textured
531 soil using tension infiltrometry. Geoderma 124, 267 – 277. doi:http://dx.doi.org/10.1016/j.geoderma.
532 2004.05.005.

533 Verbist, K., Cornelis, W.M., Gabriels, D., Alaerts, K., Soto, G., 2009. Using an inverse modelling approach
534 to evaluate the water retention in a simple water harvesting technique. HYDROLOGY AND EARTH
535 SYSTEM SCIENCES 13, 1979–1992.

Xu, X., Lewis, C., Liu, W., Albertson, J., Kiely, G., 2012. Analysis of single-ring infiltrometer data for soil hydraulic properties estimation: Comparison of best and wu methods. Agricultural Water Management 107, 34 – 41. URL: http://www.sciencedirect.com/science/article/pii/S0378377412000200, doi:https://doi.org/10.1016/j.agwat.2012.01.004.

Younes, A., Mara, T., Fahs, M., Grunberger, O., Ackerer, P., 2017. Hydraulic and transport parameter assessment using column infiltration experiments. Hydrology and Earth System Sciences 21, 2263–2275. URL: https://www.hydrol-earth-syst-sci.net/21/2263/2017/, doi:10.5194/hess-21-2263-2017.

Zou, Z.Y., Young, M., Li, Z., Wierenga, P., 2001. Estimation of depth averaged unsaturated soil hydraulic properties from infiltration experiments. Journal of Hydrology 242, 26 – 42. URL: http://www.sciencedirect.com/science/article/pii/S0022169400003851, doi:http://dx.doi.org/10.1016/S0022-1694(00)00385-1.